Received 14 June; accepted 26 November 2002; doi:10.1038/nature01331.

1. Cahn, W. J. Critical point wetting. *J. Chem. Phys.* **66,** 3667–3670 (1977).
2. Nakanishi, H. & Fisher, M. E. Multicriticality of wetting, prewetting, and surface transitions. *Phys. Rev. Lett.* **49,** 1565–1568 (1982).
3. Sheng, P. Phase transition in surface-aligned nematic films. *Phys. Rev. Lett.* **37,** 1059–1062 (1976).
4. Sluckin, T. J. & Poniewierski, A. Novel surface phase transition in nematic liquid crystals. *Phys. Rev. Lett.* **55,** 2907–2910 (1985).
5. Yokohama, H. *et al.* Boundary dependence of the formation of new phase at the isotropic-nematic transition. *Mol. Cryst. Liq. Cryst.* **99,** 39–52 (1983).
6. Clark, N. A. Surface memory effects in liquid crystals: Influence of surface composition. *Phys. Rev. Lett.* **55,** 292–295 (1985).
7. Chen, W. *et al.* Orietational wetting behavior of a liquid crystal homologous series. *Phys. Rev. Lett.* **62,** 1860–1863 (1989).
8. Miyano, K. Wall-induced pretransitional birefringence: a new tool to study boundary aligning forces in liquid crystals. *Phys. Rev. Lett.* **43,** 51–54 (1979).
9. Hsiung, H. *et al.* Wall induced orientational order of a liquid crystal in the isotropic phase—an evanescent wave ellipsometry study. *Phys. Rev. Lett.* **57,** 3065–3068 (1986).
10. De Schrijver, P. *et al.* Surface-induced pretransitional order in the isotropic phase near the isotropic-nematic phase transition. *Liq. Cryst.* **21,** 745–749 (1996).
11. Crawford, G. P. *et al.* Ordering and self-diffusion in the 1st molecular layer at a liquid-crystal polymer interface. *Phys. Rev. Lett.* **66,** 723–726 (1991).
12. Akiyama, H. *et al.* Thermal stability of magnetically-aligned nematic liquid crystal layer on nonrubbed polyimide surface. *Jpn. J. Appl. Phys.* **36,** L1204–L1206 (1997).
13. Jerome, B. Surface effects and anchoring in liquid-crystals. *Rep. Prog. Phys.* **54,** 391–451 (1991).
14. Bonn, D. & Ross, D. Wetting transitions. *Rep. Prog. Phys.* **64,** 1085–1163 (2001).
15. van Haaren, J. Wiping out dirty displays. *Nature* **411,** 29–30 (2001).
16. Chaudhari, P. *et al.* Atomic-beam alignment of inorganic materials for liquid-crystal displays. *Nature* **411,** 56–59 (2001).
17. Maret, G. & Dransfeld, K. *Strong and Ultrastrong Magnetic Fields and Their Applications* (ed. Herlach, F.) 143–204 (Springer, Berlin, 1985).
18. Jakli, A. *et al.* Rotational viscosities of polymer solutions in a low molecular weight nematic liquid crystal. *Mol. Cryst. Liq. Cryst.* **198,** 331–340 (1991).
19. de Gennes, P. G. & Prost, J. *The Physics of Liquid Crystals*, 2nd edn (Clarendon, Oxford, 1993).
20. Sheng, P. *et al.* Disordered-surface-layer transition in nematic liquid crystals. *Phys. Rev. A* **46,** 946–950 (1992).
21. Rosenblatt, C. Magnetic field dependence of the nematic-isotropic transition temperature. *Phys. Rev. A* **24,** 2236–2240 (1981).
22. Singh, S. Phase transitions in liquid crystals. *Phys. Rep.* **34,** 107–269 (2000).

Acknowledgements Part of this work was supported by the EU-TMR Network SILC and the Dutch Technology Foundation STW.

Competing interests statement The authors declare that they have no competing financial interests.

Correspondence and requests for materials should be addressed to M.I.B. (e-mail: boamfa@sci.kun.nl).

Magnitude and timing of temperature change in the Indo-Pacific warm pool during deglaciation

Katherine Visser*, Robert Thunell* & Lowell Stott†

* *Department of Geological Sciences, University of South Carolina, Columbia, South Carolina 29205, USA*
† *Department of Earth Sciences, University of Southern California, Los Angeles, California 90089, USA*

Ocean–atmosphere interactions in the tropical Pacific region have a strong influence on global heat and water vapour transport and thus constitute an important component of the climate system[1,2]. Changes in sea surface temperatures and convection in the tropical Indo-Pacific region are thought to be responsible for the interannual to decadal climate variability observed in extratropical regions[1,3], but the role of the tropics in climate changes on millennial and orbital timescales is less clear. Here we analyse oxygen isotopes and Mg/Ca ratios of foraminiferal shells from the Makassar strait in the heart of the Indo-Pacific warm pool, to obtain synchronous estimates of sea surface temperatures and ice volume. We find that sea surface temperatures increased by 3.5–4.0 °C during the last two glacial—interglacial transitions, synchronous with the global increase in atmospheric CO_2 and Antarctic warming, but the temperature increase occurred 2,000–3,000 years before the Northern Hemisphere ice sheets melted. Our observations suggest that the tropical Pacific region plays an important role in driving glacial—interglacial cycles, possibly through a system similar to how El Niño/Southern Oscillation regulates the poleward flux of heat and water vapour.

Much research in the past two decades has pointed to the North Atlantic, and its prominence in controlling thermohaline circulation, as being the key to the driving of global climate variability on both millennial and orbital timescales[4]. The small (1–2 °C) changes in sea surface temperature (SST) predicted for the tropics for the Last Glacial Maximum (LGM) by the CLIMAP[5] study also focused attention away from the tropics to the North Atlantic. However, recent studies suggest that tropical Pacific SSTs were at least 3 °C (ref. 6) and perhaps 5 °C (ref. 7) cooler during the LGM. Such changes in tropical SST should have a significant effect on the export of heat and water vapour to high latitudes, as well as atmospheric CO_2 concentrations[8]. Indeed, coupled ocean–atmosphere model studies indicate that heat flux from the tropics may be the most viable source of forcing for global climate change on both millennial and orbital timescales[9].

Establishing the timing of climate change in the tropics relative to changes in other regions is necessary in order to evaluate the role that this region plays in driving global climate change. It has been suggested that changes in atmospheric CO_2 and Southern Hemisphere temperature are synchronous, and lead Northern Hemisphere ice volume changes by several thousand years[10,11]. Conversely, it has been reported that the warming associated with the last deglaciation was synchronous between the two hemispheres[12].

We performed Mg/Ca and oxygen isotope analyses on the surface dwelling planktonic foraminifer *Globigerinoides ruber* from core MD9821-62 (4° 41.33′ S, 117° 54.17′ E; 1,855 m water depth) collected from the Makassar strait in the heart of the Indo-Pacific warm pool (IPWP; Fig. 1). This is a region of deep atmospheric convection, and the primary source of heat and water vapour flux to the atmosphere.

The $\delta^{18}O$ of *G. ruber* is a recorder of the combined effects of seawater $\delta^{18}O$ variability and the temperature at which the foraminifer calcite precipitates. The ^{18}O composition of surface waters in the western tropical Pacific records both the effects of ice volume change and local salinity variability. The Mg/Ca ratio of planktonic foraminifers is a relatively new proxy for estimating SST. The

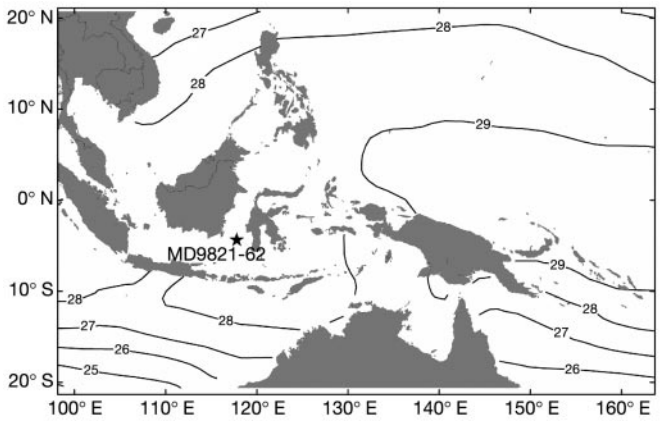

Figure 1 Map of sea surface temperature of the western Pacific and Indonesian region. The 'warm pool' is demarcated by the 28 °C isotherm. Core MD9821-62 was collected from the Makassar strait, Indonesia (4° 41.33′ S, 117° 54.17′ E, 1,855 m water depth).

temperature dependence of Mg incorporation into planktonic foraminiferal calcite has been verified both in culturing experiments[13] and field studies[14]. As the Mg/Ca of planktonic foraminifer is not influenced by the same parameters as $\delta^{18}O$, it can be used in parallel with $\delta^{18}O$ to estimate what fraction of the $\delta^{18}O$ signal is due to ice volume or local salinity changes. Additionally, by measuring Mg/Ca and $\delta^{18}O$ on the same samples we can determine the relative phasing between tropical SST change and high latitude deglaciation. To calculate SST, we used an equation[15] developed for *G. ruber* from South China Sea surface sediment samples recovered from depths less than 2,000 m: Mg/Ca (mmol mol^{-1}) = 0.38 exp[0.089 SST (°C)].

This equation has same exponential term as the equation developed by Lea *et al.*[6] for the equatorial Pacific, but differs by having a larger pre-exponential constant. It has been shown that increased dissolution decreases the pre-exponential constant[16]. This suggests that the South China Sea samples used in the Hastings *et al.*[15] calibration may have been better preserved than the tropical Pacific samples used by Lea *et al.*[6]. Several lines of evidence indicate that calcite is well preserved in our core. First, the core depth (1,855 m) is well above both the present day (~3,400 m) and glacial-age lysocline depths (~4,100 m)[17]. Second, aragonite, which dissolves more easily than calcite, is present throughout the core. Third, there is no significant difference in the average shell weight of *G. ruber* between the interglacial (11.6 and 11.1 μg per shell for marine isotope stages (MIS) 1 and 5e, respectively) and glacial periods (11.3 and 11.8 μg per shell for MIS 2 and 6, respectively). Thus, we chose to use the Hastings *et al.*[15] equation, because our core is relatively unaffected by dissolution and the estimated Holocene temperatures are very similar to modern day temperatures (~28–29 °C) at our core location.

The age model for the portion of the core that extends back through the last glacial is based on 10 accelerator mass spectrometry (AMS) ^{14}C dates that were determined on *G. ruber* and converted to calendar years. For the penultimate glacial and last interglacial (MIS 6 and 5e), the *G. ruber* $\delta^{18}O$ record was correlated to the SPECMAP stacked $\delta^{18}O$ chronology[18]. The time scale was constructed assuming constant sedimentation rates between radiocarbon dates and isotope tie points. On the basis of this age model, the average sample spacing is ~400 yr.

We used two different approaches to estimate the magnitude of the temperature changes across the last two glacial terminations from the Mg/Ca data. First, we averaged the temperatures determined for all samples within each of the glacial (MIS 2 and 6) and interglacial (MIS 1 and 5e) intervals (Fig. 2). This approach yields SST changes of 3.3 ± 0.6 °C and 4.1 ± 0.6 °C across terminations I and II, respectively, and are considered conservative estimates of the total SST change. These data also suggest that, on average, western tropical Pacific SSTs were the same during stages 2 and 6 (25.8 and 25.9 °C), and that the last interglacial was approximately 1 °C warmer than the Holocene (30.0 versus 29.1 °C) at this location. The second approach uses three consecutive samples that represent the minimum glacial and maximum interglacial temperatures, and yields temperature changes of 3.7 ± 0.6 °C and 5.3 ± 0.7 °C across terminations I and II, respectively (Fig. 2). These temperature estimates are supported by our oxygen isotope data. The amplitudes of the $\delta^{18}O$ changes across terminations I and II are 1.7‰ and 1.9‰, respectively (Fig. 2), of which 0.9‰ and 1.1‰, respectively, is attributed to the change in global ice volume[11,19]. Assuming no salinity change, this translates into a temperature change of ~3.6 °C across both terminations, using the $\delta^{18}O$–temperature relationship of 0.22‰ $\delta^{18}O \equiv 1$ °C (ref. 20). These Mg/Ca and $\delta^{18}O$ derived temperature changes are larger than those estimated by CLIMAP[5] for this region, but are in line with a growing body of evidence that

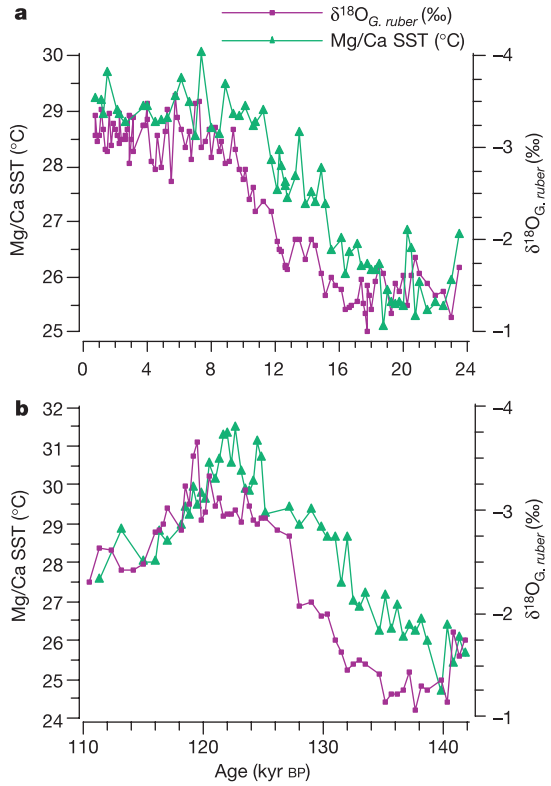

Figure 2 *Globigerinoides ruber* oxygen isotope (purple curve) and Mg/Ca SST (green curve) records for core MD9821-62 plotted versus time for MIS 1 and 2 (**a**) and MIS 5e and 6 (**b**). For both terminations, the surface temperature warming occurs several thousand years before the decrease in ice volume reflected by the $\delta^{18}O$ record.

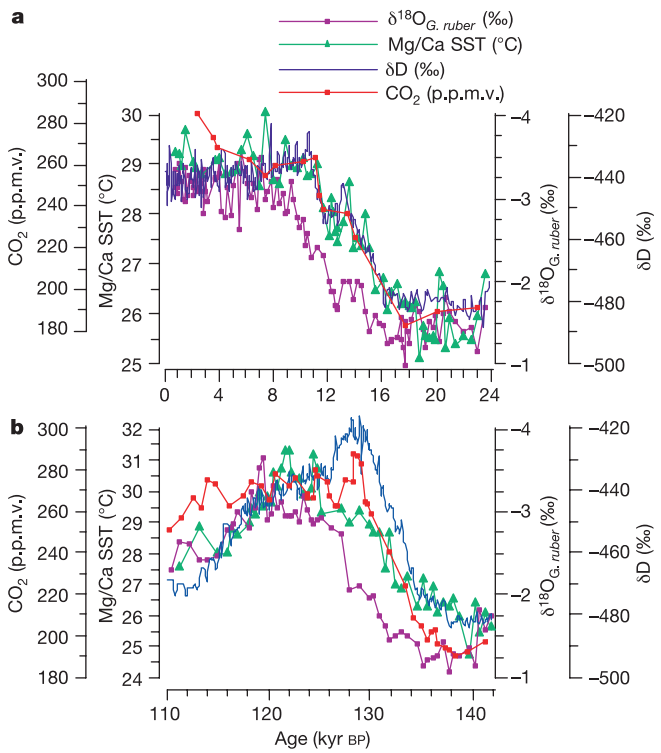

Figure 3 Comparison of the MD9821-62 *G. ruber* $\delta^{18}O$ (purple curve) and Mg/Ca SST (green curve) records with the Vostok CO_2 (red curve) and deuterium isotope (blue curve) records[22]. The deuterium record reflects changes in atmospheric temperature over Antarctica. The change in the Mg/Ca, deuterium and CO_2 records during both deglaciations occurs before the $\delta^{18}O$ change.

suggests that the tropical oceans were 3–5 °C colder during the LGM[6,7].

For both terminations, the change in Mg/Ca is not synchronous with the change in $\delta^{18}O$ (Fig. 2). As the *G. ruber* $\delta^{18}O$ record reflects both local changes in SST and global ice volume, the timing of change in the Mg/Ca and $\delta^{18}O$ records should be similar during the period of surface temperature warming associated with deglaciation. However, for both terminations, the $\delta^{18}O$ records continue to decrease for several thousand years after the Mg/Ca records indicate that SST reached interglacial values. This additional change in $\delta^{18}O$ is interpreted as reflecting the decrease in global ice volume. Within the limits of our age model, we estimate that the $\delta^{18}O$ ice volume changes lag the Mg/Ca SST changes by 2,000–3,000 yr. For example, during termination I, SST reaches the modern interglacial value of 29 °C by ~12 kyr ago, while $\delta^{18}O$ continues to decrease until at least 10 kyr ago. Our findings indicate that the tropical western Pacific region warmed before the melting of Northern Hemisphere ice sheets during the last two deglaciations. This phase relationship is consistent with that recently reported for the equatorial Pacific[6].

What are the broader implications of our findings concerning the magnitude and timing of SST change in the Indo-Pacific warm pool during the last two glacial–interglacial transitions? The global atmosphere is very sensitive to changes in tropical SST[2], particularly with regards to its effect on fluxes of heat and water vapour to higher latitudes. The tropics, in general, and the Indo-Pacific warm pool, in particular, are the main regions from which water vapour is supplied to the atmosphere. As water vapour is one of the main greenhouse gases, substantial variations in the moisture content of the atmosphere associated with past changes in SST can be expected to have had a major role in global climate change. It has been estimated that during the last glacial period the absolute water vapour content of the atmosphere at sea level in the tropics was 70% of the modern value, and that the greenhouse effect of this decrease in water vapour led to a global cooling of 2 °C (ref. 21). Similarly, a decrease in tropical Indo-Pacific SST during glacial periods of 3.5–5 °C should contribute to the 80 p.p.m. decrease in atmospheric CO_2 concentration recorded in ice cores[22], owing to the fact that CO_2 is more soluble in colder water. For a 1 °C increase in temperature, the equilibrium partial pressure of CO_2 exerted by sea water increases by ~11–16 p.p.m. (ref. 8). Therefore, a 3.5 °C cooling in the tropics could account for a substantial portion of the atmospheric decrease in CO_2 during glacial periods, suggesting that the low latitude oceans have a significant effect on atmospheric CO_2 concentrations. Indeed, the changes in atmospheric CO_2 are synchronous with our estimated SST changes in the Indo-Pacific for the last two terminations (Fig. 3).

The fact that SST change leads the ice volume change by 2,000–3,000 yr during the past two terminations at our study site supports the notion that the tropical Pacific is actively involved in forcing global climate change[1,2,9]. As noted previously[6], the increase in SST in the tropical Pacific during deglaciation is synchronous with an increase in the Vostok ice-core deuterium isotope record[22], which reflects atmospheric warming over Antarctica (Fig. 3). The present day pattern of meridional heat transport by the oceans and atmosphere may provide some insight into the mechanism that links climate change in the tropical Pacific and the high southern latitudes. At present, the patterns of surface heat transport are quite different between the Atlantic and Pacific oceans. In the Atlantic, heat moves northward at all latitudes and results in cross-equatorial heat transport. By contrast, the tropical Pacific transports heat to both hemispheres, although this export is asymmetrical in that roughly twice as much heat is directed to the south than the north[23].

We suggest that past changes in the transport of heat to the high southern latitudes may have been regulated by a system analogous to the El Niño/Southern Oscillation (ENSO). Present day variability in SST, sea-ice extent, and wind stress in the Antarctic region is tied, via atmospheric teleconnections, to tropical Pacific ENSO activity[24]. Recent work suggests that the tropical Pacific was dominated by an El Niño-like climate during the LGM[25]. This would have decreased convection in the western Pacific, and reduced both zonal and meridional circulation. Conversely, a switch to La Niña-like conditions occurred during deglaciation[25,26], and reinvigorated heat transport to the high southern latitudes.

Additionally, the warming of surface waters in these regions during deglaciation would have resulted in a flux of CO_2 to the atmosphere, which would have had a positive feedback on global warming. A new view of the importance of the tropics in controlling global climate change is beginning to emerge, although the nature of the linkage between tropical and extra-tropical regions still needs to be resolved. □

Methods

Oxygen isotope analyses

These were conducted on specimens (60–70 μg) of the planktonic foraminifer *G. ruber* picked from the 250–355 μm size fraction. Analyses were carried out using a VG Optima stable isotope ratio mass spectrometer (IRMS) equipped with an automated carbonate system. The samples were reacted in a common acid bath of 100% phosphoric acid at 90 °C. The evolved CO_2 gas was then analysed on the IRMS. Oxygen and carbon isotopic data are reported in delta notation relative to (Vienna) Pee Dee Belemnite. The long-term standard reproducibility for oxygen ($\delta^{18}O$) isotopes based on replicate measurements of a reference standard is ±0.07‰.

Mg/Ca analyses

The Mg/Ca ratio in *G. ruber* was determined on a Jobin-Yvon Ultima inductively coupled plasma-atomic emission spectrophotometer (ICP-AES). For this study, the two lines used were: Ca (317.93 nm wavelengths) and Mg (285.213 nm). Approximately 220–240 μg (~23 shells from the 250–355 μm size fraction) of precleaned (in methanol) whole foraminifers were processed using the following procedure first developed by Boyle[27]. First, the samples were gently crushed in acid-cleaned 1.5-ml microcentrifuge tubes, making sure that all chambers were fully open. In order to remove the fine clays, the foraminifer fragments were covered with deionized water (DI H_2O), sonicated for ~1 min, resuspended by the addition of 400 μl DI H_2O; then the supernatant was siphoned off using a micropipette. These steps were repeated twice with DI H_2O, twice with methanol, and then once with DI H_2O to remove the methanol. To remove organic matter, 250 μl of an oxidizing reagent (0.1 N NaOH and 0.15% H_2O_2) was added. The samples were capped and placed in a boiling water bath for 5 min, sonicated for 1 min, then replaced in the boiling water bath for 5 min. Afterwards, the oxidizing solution was removed, and the samples were rinsed twice with 400 μl of DI H_2O to ensure complete removal of the oxidizing agent. The samples were then transferred to new, acid-cleaned microcentrifuge tubes. The cleaned shells were leached with weak acid (0.001 M HNO_3) and rinsed with DI H_2O. Finally, ~500 μl of 5% HNO_3 was added to dissolve the foraminifer shells. It is estimated that ~40–60% of the initial sample weight was lost through the cleaning procedure. The *G. ruber* Mg/Ca equation developed by Hastings *et al.*[15] has the same exponential and pre-exponential constants as the equation recently presented by Dekens *et al.*[28] The difference between the two equations lies in the fact that the latter equation has an added term for water depth. The Hastings *et al.*[15] equation is used in this study because it yields Holocene temperatures that are consistent with present day temperatures at our core location. The standard error of estimate for the various temperature equations derived from core top calibrations is typically in the range of 0.5–1.0 °C (refs 6, 14, 15, 28).

Calibration of radiocarbon dates

AMS ^{14}C dates were determined on monospecific samples (4–10 mg) of the planktonic foraminifer *G. ruber* at the Center for Accelerator Mass Spectrometry, Lawrence Livermore National Laboratory. The youngest eight ^{14}C ages were converted to calendar ages using the calibration program CALIB 4.3 (ref. 29) and the oldest two ^{14}C ages were converted using the equation $(-698.65 \times 10^{-3} + 1.2695(^{14}Cc) - [2.7039 \times 10^{-6}(^{14}Cc)^2])$ (we find $r^2 = 0.999$; standard error = ±150 yr), where ^{14}Cc is the reservoir-corrected ^{14}C age[30]. In order to account for the difference in ^{14}C composition between the atmosphere and the surface ocean, a reservoir correction of 400 yr was subtracted from the ^{14}C dates before converting them to calendar years[31].

Received 7 May; accepted 5 November 2002; doi:10.1038/nature01297.

1. Cane, M. A role for the tropical Pacific. *Science* **282,** 59–61 (1998).
2. Pierrehumbert, R. Climate change and the tropical Pacific: The sleeping dragon wakes. *Proc. Natl Acad. Sci.* **97,** 1355–1358 (2000).
3. Hoerling, M., Hurrell, J. & Xu, T. Tropical origins for recent North Atlantic climate change. *Science* **292,** 90–92 (2001).
4. Broecker, W. Paleocean circulation during the last deglaciation: a bipolar seesaw? *Paleoceanography* **13,** 119–121 (1998).
5. CLIMAP Project Members. Seasonal reconstructions of the Earth's surface at the last glacial maximum. *Geol. Soc. Am. Map Chart Ser.* **MC-36,** 1–18 (1981).
6. Lea, D., Pak, D. & Spero, H. Climate impact of late Quaternary equatorial Pacific sea surface temperature variations. *Science* **289,** 1719–1924 (2000).
7. Guilderson, T., Fairbanks, R. & Rubenstone, J. Tropical Atlantic coral oxygen isotopes; glacial-interglacial sea surface temperatures and climate change. *Mar. Geol.* **172,** 75–89 (2001).

8. Bacastow, R. The effect of temperature change of the warm surface waters of the oceans on atmospheric CO_2. *Glob. Biogeochem. Cycles* **10,** 319–333 (1996).
9. Cane, M. & Clement, A. *Mechanisms of Global Climate Change at Millennial Time Scales* AGU Geophysical Monograph 112 (eds Clark, P., Webb, R. & Keigwin, L.) 373–383 (American Geophysical Union, Washington DC, 1999).
10. Broecker, W. & Henderson, G. The sequence of events surrounding Termination II and their implications for the cause of glacial-interglacial CO_2 changes. *Paleoceanography* **13,** 352–364 (1998).
11. Shackleton, N. The 100,000-year ice age cycle identified and found to lag temperature, carbon dioxide, and orbital eccentricity. *Science* **289,** 1897–1902 (2000).
12. Steig, E. *et al.* Synchronous climate changes in Antarctica and the North Atlantic. *Science* **282,** 92–95 (1998).
13. Lea, D., Mashiotta, T. & Spero, H. Controls on magnesium and strontium uptake in planktonic foraminifer determined by live culture. *Geochim. Cosmochim. Acta* **63,** 2369–2379 (1999).
14. Elderfield, H. & Ganssen, G. Past temperature and $\delta^{18}O$ of surface ocean waters inferred from foraminiferal Mg/Ca ratios. *Nature* **405,** 442–445 (2000).
15. Hastings, D., Kienast, M., Steinke, S. & Whitko, A. A Comparison of three independent paleotemperature estimates from a high resolution record of deglacial SST records in the tropical South China Sea. *Eos* **82,** PP12B-10 (2001).
16. Rosenthal, Y., Lohmann, G., Lohmann, K. & Sherrell, R. Incorporation and preservation of Mg in *Globigerinoides sacculifer*: Implications for reconstructing the temperature and $^{18}O/^{16}O$ of seawater. *Paleoceanography* **15,** 135–145 (2000).
17. Farrell, J. & Prell, W. Climatic change and $CaCO_3$ preservation: An 800,00 year bathymetric reconstruction from the central equatorial Pacific Ocean. *Paleoceanography* **4,** 447–466 (1989).
18. Martinson, D. *et al.* Age dating and the orbital theory of the ice-ages: development of a high-resolution 0-300,000 year chronostratigraphy. *Quat. Res.* **27,** 1–29 (1987).
19. Schrag, D., Hampt, G. & Murray, D. Pore fluid constraints on the temperature and oxygen isotopic composition of the glacial ocean. *Science* **272,** 1930–1932 (1996).
20. Epstein, S., Buchsbaum, R., Lowenstam, H. & Urey, H. Revised carbonate-water isotopic temperature scale. *Geol. Soc. Am. Bull.* **64,** 1315–1325 (1953).
21. Broecker, W. Mountain glaciers: Recorders of atmospheric water vapor content. *Glob. Biogeochem. Cycles* **11,** 589–597 (1997).
22. Petit, J. *et al.* Climate and atmospheric history of the past 420,000 years from the Vostok ice core, Antarctica. *Nature* **399,** 429–436 (1999).
23. Hastenrath, S. On meridional heat transports in the world ocean. *J. Phys. Ocean.* **12,** 922–927 (1982).
24. White, W. B. & Peterson, R. An Antarctic circumpolar wave in surface pressure, wind, temperature and sea-ice extent. *Nature* **380,** 699–702 (1996).
25. Koutavas, A., Lybch-Stieglitz, J., Marchitto, T. M. & Sachs, J. El Niño-like pattern in ice age tropical Pacific sea surface temperature. *Science* **297,** 226–230 (2002).
26. Stott, L., Poulsen, C., Lund, S. & Thunell, R. Super ENSO and global climate oscillations at millennial time scales. *Science* **297,** 222–226 (2002).
27. Boyle, E., Labeyrie, L. & Duplessy, J-C. Calcitic foraminiferal data confirmed by cadmium in aragonitic *Hoeglundina*; application to the last glacial maximum in the northern Indian Ocean. *Paleoceanography* **10,** 881–900 (1995).
28. Dekens, P. S., Lea, D., Pak, D. & Spero, H. Core top calibration of Mg/Ca in tropical foraminifer: Refining paleotemperature estimation. *Geochem. Geophys. Geosyst.* **3,** 10.1029/2001GC000200 (2002).
29. Stuiver, M. *et al.* INTCAL98 Radiocarbon age calibration 24,000 - 0 cal BP. *Radiocarbon* **40,** 1041–1083 (1998).
30. Guilderson, T., Burckle, L., Hemming, S. & Peltier, W. Late Pleistocene sea level variations derived from the Argentine Shelf. *Geochem. Geophys. Geosyst.* **1,** 10.1029/2000GC000098 (2000).
31. Bard, E. Correction of accelerator mass spectrometry ^{14}C ages measured in planktonic foraminifer: Paleoceanographic implications. *Paleoceanography* **3,** 635–645 (1988).

Acknowledgements We thank E. Tappa for technical assistance. This work was supported by the US National Science Foundation (R.T. and L.S.).

Competing interests statement The authors declare that they have no competing financial interests.

Correspondence and requests for materials should be addressed to R.T. (e-mail: thunell@geol.sc.edu)

Group decision-making in animals

L. Conradt & T. J. Roper

School of Biological Sciences, University of Sussex, Brighton BN1 9QG, UK

Groups of animals often need to make communal decisions, for example about which activities to perform[1], when to perform them[2–9] and which direction to travel in[1,6,7]; however, little is known about how they do so[10–12]. Here, we model the fitness consequences of two possible decision-making mechanisms: 'despotism'[6,7,10] and 'democracy'[1,6,7,10]. We show that under most conditions, the costs to subordinate group members, and to the group as a whole, are considerably higher for despotic than for democratic decisions. Even when the despot is the most experienced group member, it only pays other members to accept its decision when group size is small and the difference in information is large. Democratic decisions are more beneficial primarily because they tend to produce less extreme decisions, rather than because each individual has an influence on the decision *per se*. Our model suggests that democracy should be widespread and makes quantitative, testable predictions about group decision-making in non-humans.

Notwithstanding extensive literature on decision-making by animals acting alone[13–15], group decision-making processes have been largely neglected from a theoretical point of view[6,7,10]. Two extreme mechanisms whereby a group could in principle reach communal decisions are: (1) despotically, where one dominant decides; and (2) democratically, where a majority of group members decides. The relative fitness consequences of these mechanisms are unknown. Many authors have assumed despotism without testing[6,7,10], because the feasibility of democracy, which requires the ability to vote and to count votes, is not immediately obvious in non-humans. However, empirical examples of 'voting' behaviours include the use of specific body postures[1,10,11], ritualized movements[6,7,9,11,16], and specific vocalizations[5,8,12], whereas 'counting of votes' includes adding-up to a majority of cast votes[5–8,11], integration of voting signals until an intensity threshold is reached[9,16] and averaging over all votes[1,12,16] (Table 1). Thus, democracy may exist in a range of taxa and does not require advanced cognitive capacity. Here, we model the fitness consequences of despotic and democratic decisions. One important context in which social animals frequently have to make communal decisions is in the duration of group activities[1–7,17]. This 'activity synchronization' is essential if a group is to remain spatially coherent[1–7,10]. However, to reach consensus decisions about the duration of activities, group members often have to compromise their own optimal activity budgets[1,3,18,19], the costs of which (synchronization costs) can be an important factor in shaping the social organization of populations[1–4,17]. Our model compares the synchronization costs of despotic and democratic groups.

The model in Box 1 shows that synchronization costs are usually higher for despotic than for democratic groups. However, if synchronization costs are asymmetric (that is, stopping too late costs less than stopping too early, or vice versa), a modified democratic decision is least costly. In this case, the decision should be based not on a 50% majority, but on a proportion of members that depends on the degree of asymmetry in costs. For example, if stopping too early is twice as costly as stopping too late, the group

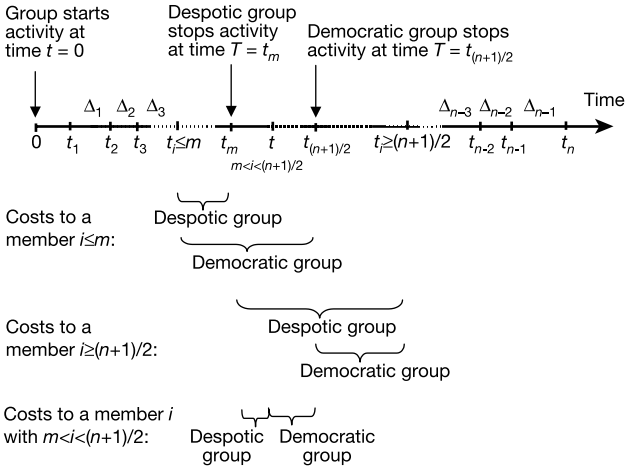

Figure 1 Scheme of a despotic or democratic decision about the duration of a single group activity session, and resulting costs. (See Box 1 for definitions.)